Chemical Physics Letters 465 (2008) 220–225

Contents lists available at ScienceDirect

Chemical Physics Letters

journal homepage: www.elsevier.com/locate/cplett

Structure and stability of aluminium trihydroxides bayerite and gibbsite: A quantum mechanical *ab initio* study with the CRYSTAL06 code

Raffaella Demichelis [a,*], Bartolomeo Civalleri [a,b], Yves Noel [c], Alessio Meyer [a], Roberto Dovesi [a,b]

[a] Dipartimento di Chimica IFM, Università di Torino, Via P. Giuria 7, 10125 Torino, Italy
[b] NIS – Nanostructured Interfaces and Surfaces – Centre of Excellence, Via P. Giuria 7, 10125 Torino, Italy
[c] Université Pierre et Marie Curie-Paris6, UMR 7160, Lab. PMMP, Paris 75005, France

ARTICLE INFO

Article history:
Received 8 August 2008
In final form 25 September 2008
Available online 1 October 2008

ABSTRACT

The structure and energetics of bayerite and gibbsite have been investigated at the periodic *ab-initio* quantum-mechanical level by using a Gaussian type basis set and the B3LYP Hamiltonian.

Both systems have layered structure, with intra-layer and inter-layer hydrogen bonds (HBs). In gibbsite the latter are stronger than in bayerite: 23.15 and 17.59 kJ/mol, respectively. The formation Gibbs free energy has been calculated, including entropic and enthalpic contributions: at 298 K gibbsite is more stable than bayerite by 7.74 kJ/mol.

1. Introduction

Aluminium trihydroxides ($Al_2O_3 \cdot 3H_2O$) belong to the wide family of aluminium hydroxides ($Al_2O_3 \cdot nH_2O$, n being the hydration degree) [1–3]. In industry, they are used as main components in antacid drugs [4], as alumina catalysts precursors [1], as adsorbants in chromatography and manufacturing of several materials [4].

Four polymorphs corresponding to the Al trihydroxide unit formula have been found by experiments, namely gibbsite (in 1820 [5]), or γ-$Al(OH)_3$ (also known as hidrargillite), bayerite (in 1925 [6]), or α-$Al(OH)_3$, nordstrandite (in 1956 [7]) and doyleite (in 1985 [8]). Gibbsite is the most diffuse in natural ores; bayerite is less diffuse, but can easily be synthesized [9]; both occupy a very important role in the aluminium industry [10,11].

The four polymorphs share several common features: they all do have a layered structure, where each layer consists of a double layer of OH ions, with Al^{3+} cations occupying two thirds of the octahedral cavities, so that the OH double-layer can be represented with a sheet of $Al(OH)_6$ octahedra sharing edges. Within each layer, large triangular-hexagonal cavities are present. The cohesion among different layers is ensured by inter-layer hydrogen bonds (HB). Two are the main differences among these system: the sequence of the layers and the orientation of the O–H bonds. The Al–O frame within a sheet is extremely similar in all cases.

Many experiments have been devoted to the study of the structural, dynamical and thermodynamical properties of bayerite and gibbsite. In the last few years force-field simulations [12,13] and quantum-mechanical *ab-initio* studies based on density functional theory (DFT) [4,14–19] have been carried out, aimed to determine the structure, the relative stability and other properties of the considered systems. The OH stretching frequencies of bayerite and gibbsite have also been calculated [14,16,19].

In the present paper, we use a quantum mechanical periodic approach based on an all-electron Gaussian-type basis set and the hybrid B3LYP [20] Hamiltonian, as implemented in the CRYSTAL06 code [21], for the study of the structure and the relative stability of bayerite and gibbsite. Such a method has already been applied for the study of the aluminium monohydroxides ($n = 1$), namely diaspore [1] and boehmite [2], and of akdalaite [3] ($n = 0.2$).

Differences and similarities between the structures of the two polymorphs have been investigated. The inter-layer HB pattern, as well as the sequence by which the layers are repeated and their influence on the stability of the systems have been analyzed. The isolated two dimensional slab model has been compared with the 3D crystal, in order to elucidate the inter-layer energetics.

The full vibrational spectrum of bayerite and gibbsite has been computed, in order to obtain the zero point energy (ZPE), the entropic and enthalpic thermal contributions to the Gibbs energy as a function of temperature. Such contributions were disregarded in previous studies [15,17], where the Gibbs energy of the solid systems had been approximated to the electronic energy only. The Gibbs free energy associated to the dehydration reaction has been estimated as a function of temperature, and the results obtained at 298 K have been compared with experiments.

2. Computational details

The present calculations have been performed with CRYSTAL06 [21], a periodic *ab-initio* all electron program that uses a Gaussian type functions (GTF) basis set.

* Corresponding author. Fax: +39 011 670 7855.
E-mail address: raffaella.demichelis@unito.it (R. Demichelis).
URL: http://www.nis.unito.it (R. Dovesi).

0009-2614/$ - see front matter © 2008 Elsevier B.V. All rights reserved.
doi:10.1016/j.cplett.2008.09.070

For Al, O and H, all-electron 8-621G(d), 8-411G(d) and 211G(p) contractions, already used in previous calculation [1–3,22–24], have been adopted.

The B3LYP [20] Hamiltonian, widely and successfully used in molecular quantum chemistry, as well as in solid state calculations has been adopted. It has been shown to provide excellent results for geometries and vibrational frequencies, superior to the ones obtained with LDA or GGA type functionals [25–28]. See [1,29] for a discussion of its performances in the special case of the OH stretching.

The level of accuracy in evaluating the Coulomb and Hartree-Fock exchange series is controlled by five parameters [21], for which the 7 7 7 7 14 values have been selected. The threshold on the SCF energy is at 10^{-8} Ha. The reciprocal space was sampled according to a regular sublattice with shrinking factor 6 [21], corresponding to the choice of 80 independent **k** vectors in the irreducible Brillouin zone. The gradient with respect to the atomic and cell coordinates is evaluated analytically [30–32] and equilibrium atomic positions are determined by using the Broyden-Fletcher-Goldfarb-Shanno scheme for Hessian updating [33–36].

The DFT exchange-correlation contribution is evaluated by numerical integration over the unit cell volume. The accuracy in the integration can be estimated by quoting the error in the integrated electronic charge density in the unit cell: $\Delta_e \simeq 1 \cdot 10^{-4}\ |e|$ for a total of 320 electrons. Further information about the grid generation and its influence on the accuracy and cost of calculation can be found in Refs. [26,27,29].

The harmonic vibrational frequencies at the Γ point have been calculated; they permit to estimate the OH and the HB strength and to calculate the ZPE, the enthalpic and the entropic contributions to the Gibbs energy. We refer to Ref. [25] for more details.

The inter-layer interaction has been estimated by using as a reference the isolated two dimensional slab model and correcting the basis set superposition error (BSSE) with the counterpoise method [37].

Manipulation and visualisation of structures have been performed with the MOLDRAW program (http://www.moldraw.unito.it) and the Jmol 3D engine (http://jmol.sourceforge.net/). Molecular drawings have been rendered with the Inkscape program (http://www.inkscape.org) using input files prepared with Jmol.

3. Structure

Bayerite (B from now on) and gibbsite (G) have a layered structure. A single sheet of $Al(OH)_6$ is shown in Fig. 1a, corresponding to the view along the *c* cell parameter (almost lying along the *z* Cartesian axis, as $\beta \simeq 90^\circ$, see below). A sort of 'triangular–hexagonal' cavity can be identified, that repeats periodically as indicated in the figure. Each vertex is shared by two octahedra, and each octahedron shares only three out of twelve edges with other octahedra. Hydrogen atoms are at both sides of the sheet; some of them point inside the triangular cavities.

B and G exhibit the same stoichiometry and space group ($P2_1/n$). The unit cells contain 56 atoms ($8Al(OH)_3$ groups, two of which form the irreducible unit), are monoclinic, with $\beta \simeq 90^\circ$ (90.3° for B and 94.6° for G as obtained by experiment, see Table 1). The *c* cell parameters are similar (9.42 Å for B and 9.74 Å for G). The other unit cell sides are even more similar, once *a* and *b* of G are exchanged in B: $a = 5.06$ Å and $b = 8.67$ Å in B, and $a = 8.68$ Å and $b = 5.09$ Å in G. The difference between the two structures is due to the HB pattern and the oxygen layer stacking.

Table 1 reports the main structural features of both systems. The most accurate experimental determinations are due to Zigan et al. [38] for B (neutron diffraction on deuterated powder samples at room temperature and 4 K) and to Saalfeld and Wedde [39] for G (X-ray diffraction, single crystal). In the former, H atom positions are determined with high accuracy, whereas in the latter, due to the well known XRD problems in locating the H atoms, O–H distances much shorter than the usual ones are observed. Table 1 documents the good agreement between the simulation and the experiment. Differences with respect to previous simulations [14–16,19] are mainly due to the different DFT schemes adopted for the calculations. In the following, numbers and figures refer to the calculated structures.

The irreducible units are shown in Fig. 1b and c. In both systems, three out of six OH groups, $(O–H)_{(4,5,6)}$, lie approximatively in the *xy* plane, and so they point towards the cavities shown in Fig. 1a; they will be indicated, in the following, as *intra-layer* OH groups. The three other OH groups, $(O–H)_{(1,2,3)}$, are oriented along the *z* axis, and will be indicated as *inter-layer* OH groups. Oxygen atoms of the intra-layer OH groups are acceptors of the inter-layer HBs and *vice versa*, the exception being $O_{(3)}$, that is not involved in any HB (note the *x* columns in Table 2: $O_{(3)}$ does not appear, the distance with the nearest H atom, *i.e.* $H_{(1)}$, being 2.6 Å). All the H atoms in B and G are involved in HB, the exception being $H_{(6)}$ in B (the nearest oxygen atom is at 2.47 Å). Table 2 and Figs. 2 and 3 summarize the features of the O–H- - -O bonds pattern.

Fig. 2 schematizes the *intra-layer* HB pattern. Note that $O_{(2)}$ in G is the acceptor of two intra-layer HB (see Table 2). For this reason the $(OH)_{(2)}$ bond distance in G is the largest one and its vibrational frequency the lowest one. A similar trends is obtained for B, where the distance between $H_{(6)}$ and $O_{(2)}$ is relatively small (but much larger than HBs), so that a weak interaction between the two atoms occurs. For the same reason, the $(OH)_{(6)}$ bond distance is very small in B, and its stretching frequency is the highest one, at 3837 cm^{-1}. Overall, intra-layer HB distances are shorter in G (2.04–2.29 Å) than in B (2.13–2.29 Å), and the corresponding OH stretching frequencies are higher in B than in G by 50–70 cm^{-1} (see Table 2).

Due to the different stacking of oxygen planes shown in Fig. 3, the *inter-layer* OH groups in B bend by about 15–20° towards the *xy* plane, whereas in G the O–H bonds are aligned along the *z* direction (90 ± 5° is the angle between O–H and the *xy* plane). As a consequence, the distance between two subsequent octahedra sheets is smaller in B than in G (see Fig. 3: 4.79 Å vs. 4.84–4.94 Å) and the inter-layer HBs of G, ranging from 1.81 to 1.93 Å, are shorter (and then stronger) than the ones of B (2.00–2.03 Å); the corresponding H- - -O–H angles ranges from 166 to 170° in G and from 168 to 175° in B. The OH stretching frequencies are lower in G (3526–3579 cm^{-1}) than in B (3568–3647 cm^{-1}), confirming that HBs are stronger in G. Note that inter-layer HBs are in both systems shorter than intra-layer HBs, and that both intra and inter-layer HBs are stronger in G than in B.

4. The inter-layer interaction

An overall estimate of the inter-layer interaction and, then, of the inter-layer HB strength, can be obtained by separating to infinite distance the individual layers. The geometry of the isolated B and G layers has been optimized: as expected, the intra-layer rearrangement is very small.

The electronic energy difference between the bulk and the single slab (corrected for the BSSE [37]) is −50.33 (B) and −67.00 (G) kJ/mol per Al_2O_3 unit. The calculation has been repeated with a higher quality basis set for H and O (TZP [40]), obtaining very similar results: −52.78 (B) and −69.45 (G) kJ/mol per Al_2O_3 unit (−211.12 and −277.80 kJ/mol per cell, respectively). Twelve out of 24 H atoms in the unit cell are involved in inter-layer HBs, so

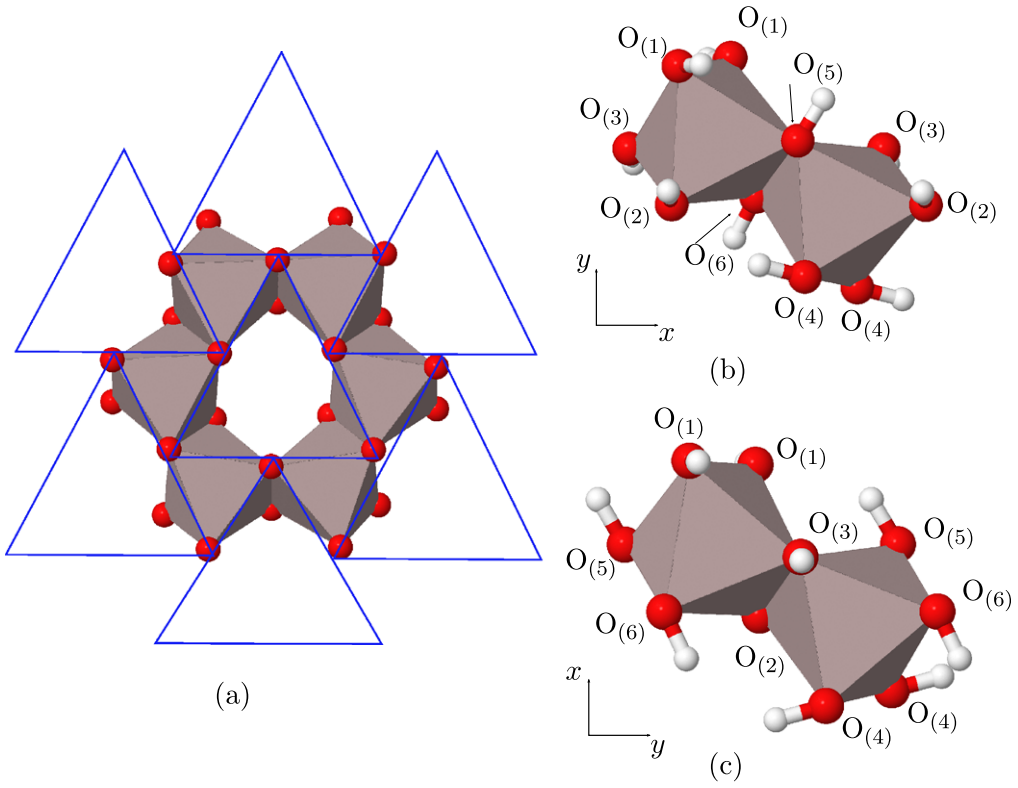

Fig. 1. (a) The single AlO_6 octahedra sheet in aluminium trihydroxides. The triangular-hexagonal cavity is shown, that repeats periodically. Octahedra in grey, oxygen atoms in red, hydrogen atoms are not shown. (b) Bayerite and (c) gibbsite irreducible units; the view along the *z* axis permits to see H atoms (in white) pointing towards intra-layer (*xy* plane) or inter-layer (*z* direction) oxygen atoms. H atoms are attributed the same label as the nearest O atom. (For interpretation of the references to colour in this figure legend, the reader is referred to the web version of this article.)

Table 1
Calculated and experimental structures of bayerite [38] and gibbsite [39]

	Bayerite		Gibbsite	
	Calculated	Experimental [38]	Calculated	Experimental [39]
a	5.1123	5.0626	8.7523	8.684
b	8.7791	8.6719	5.1138	5.078
c	9.5736	9.4254	9.7802	9.736
β	90.276	90.261	92.073	94.54
Vol.	429.67	413.80	437.45	427.98
O–H inter	0.9750	0.978	0.9768	*0.84*
O–H intra	0.9676	0.950	0.9700	*0.82*
HB inter	2.0167	1.986	1.8730	*2.09*
HB intra	2.2175	2.191	2.1981	*2.24*
Al–O_{max}	1.9619	1.943	1.937	1.947
Al–O_{min}	1.8698	1.855	1.841	1.831
Al–O_{av}	1.9168	1.904	1.918	1.904

The experimental parameters involving H atoms are emphasized for gibbsite: HB are overestimated and O–H underestimated (see text). max: maximum; min: minimum; av: averaged. 'intra' and 'inter' indicate intra-layer and inter-layer O–H and HB, respectively. Distances in Å, angles in degrees.

that, dividing by 12 the above energies, an inter-layer mean HB binding energy of 17.59 (B) and 23.15 (G) kJ/mol is obtained.

The weaker inter-layer interaction in B is the reason for the slightly larger B3LYP [20] overestimation of the *c* lattice parameter in B than in G (*i.e.* 9.57 vs. 9.42 Å in B and 9.78 vs. 9.74 Å in G, see Table 1). The B3LYP [20] overestimation of the lattice parameters is a known feature of this functional, that leads to slightly underestimated HB energies and slightly too large HB distances [41–43].The B3LYP [20] electronic energy difference between B and G per Al_2O_3 unit, ΔE_{el}, is 9.88 kJ/mol, with G being the most stable polymorph. As a cross check, calculations have been repeated with the PBE [44] functional, that tends to underestimate, rather than overestimate, HB distances, obtaining $\Delta E_{el} = 11.50$ kJ/mol, a value quite close then to the B3LYP [20] result.

5. Thermodynamic stability

In order to carry out a comparison between B and G at a temperature *T* different from 0 K, the previous numbers, referring to the electronic energy (E_{el}) only, must be corrected for the ZPE, the entropy ($\mathscr{S}(T)$) and the thermal energy ($\mathscr{H}^{0,T}(T)$) necessary to heat the system from 0 K to *T*. These thermodynamic functions can be obtained, once the phonon spectrum is known, by summing the contributions of the vibrational modes at the various points of the first Brillouin zone [21]. In the present case, only the Γ point has been considered in the sum. The error introduced with this approximation can however be considered negligible because the unit cell of both systems (a) is large, with a consequent small reciprocal space dispersion and (b) contain the same number of atoms (56), so that the error due to dispersion is expected to cancel nearly exactly when performing the difference between the two systems for the various thermodynamic functions.

The Gibbs free energy of a system can be written as

$$\mathscr{G}(T) = E_{el} + ZPE + \mathscr{H}^{0,T}(T) + PV - T\mathscr{S}(T) \quad (1)$$

The *PV* (pressure· volume) contribution is negligible for solids at room pressure.

The various contributions for B and G are given in Table 3, whose last column provides the term by term differences. As expected, all the contributions to $\mathscr{G}(T)$ are very similar for B and G, and $\Delta\mathscr{G}(298)$ is just slightly smaller than ΔE_{el} ($\Delta\mathscr{G}(298) = 7.74$

Table 2
Geometry around the six irreducible H atoms in bayerite and gibbsite

Bond	Bayerite				Gibbsite			
	O–H	H- - -O_x	x	ω	O–H	H- - -O_x	x	ω
$(O–H)_{(1)}$	0.9750	1.999	4(inter)	3621	0.9752	1.876	4(inter)	3579
$(O–H)_{(2)}$	0.9769	2.019	6(inter)	3568	0.9794	1.933	5(inter)	3526
$(O–H)_{(3)}$	0.9731	2.032	5(inter)	3647	0.9760	1.810	6(inter)	3545
$(O–H)_{(4)}$	0.9695	2.137	2(intra)	3717	0.9715	2.045	2(intra)	3656
$(O–H)_{(5)}$	0.9704	2.298	1(intra)	3727	0.9725	2.260	1(intra)	3679
$(O–H)_{(6)}$	0.9630	(2.468)	2(intra)	3837	0.9662	2.289	2(intra)	3767

The calculated OH and HB distances (in Å) are given; x is the label of the oxygen atom involved in the HB, 'inter' and 'intra' refer to the direction of the HB (in the xy plane or along the z axis, respectively). In the last column, the harmonic stretching frequency of each OH group is shown (ω, cm^{-1}). Note in the x columns that $O_{(3)}$ is never involved in HB.

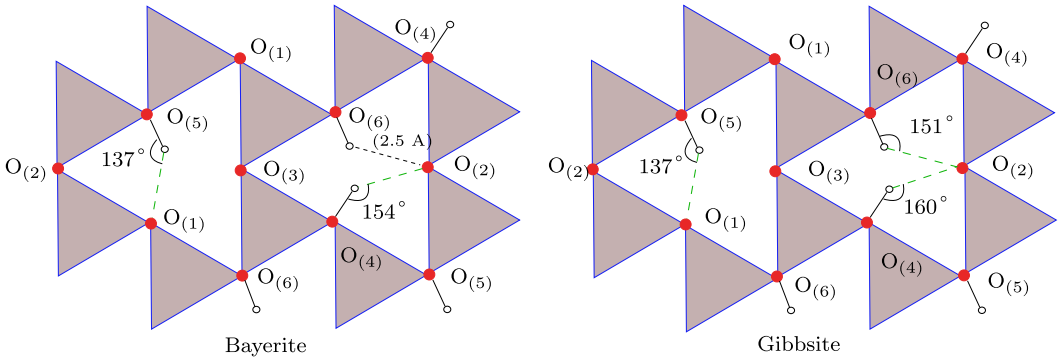

Fig. 2. Intra-layer pattern of H atoms in bayerite and gibbsite. The scheme represents the octahedra frame on the xy plane, as shown in Fig. 1. HBs are in green dashed lines. Note that two different triangular cavities are present. (For interpretation of the references to colour in this figure legend, the reader is referred to the web version of this article.)

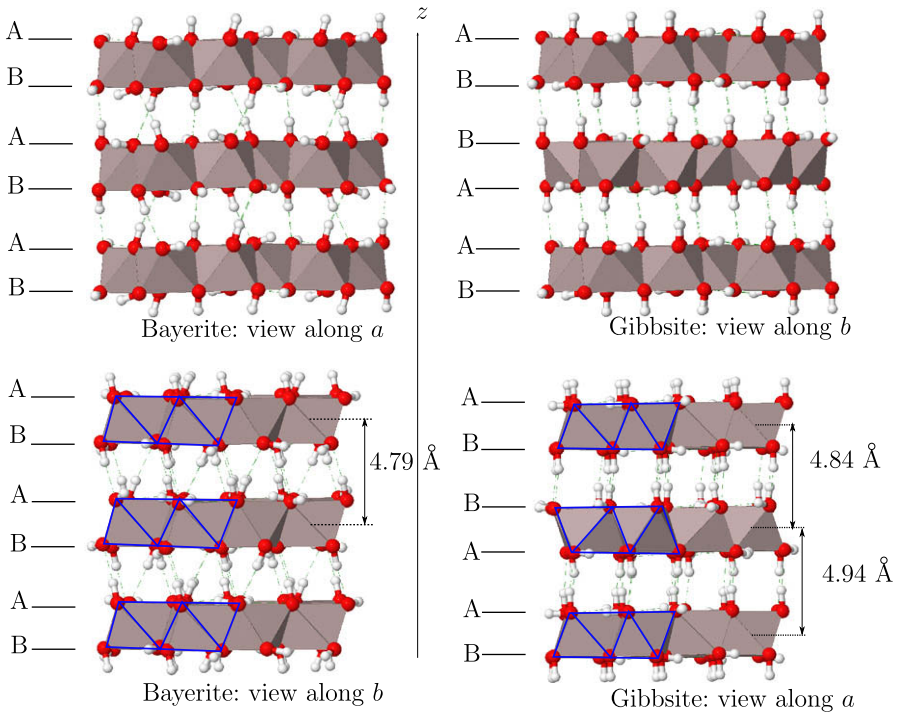

Fig. 3. Bayerite and gibbsite oxygen planes stacking: view along the a and b cell parameters. The shape of the octahedra sheets stacking is shown with blue lines in the bottom figures.

kJ/mol, $\Delta E_{el} = 9.88$ kJ/mol), and slowly decreases with T ($\Delta\mathscr{G}(373.2) = 7.36$ kJ/mol). This result is in good agreement with the experimental values at 298 K, ranging from 4.0 to 10.58 kJ/mol [10,45,46]. The difference calculated by Digne et al. [15] is 10.7 kJ/mol.

We can then estimate $\Delta\mathscr{G}(T)$ for the hydration reaction

$$\alpha\text{-}Al_2O_3 + 3H_2O \rightleftharpoons Al_2O_3 \cdot 3H_2O \quad (2)$$

and T_{inv}, the temperature at which the Al_2O_3 + $3H_2O$ phases become more stable than B and G ($\Delta\mathscr{G} = 0$).

Table 3
Contributions to the Gibbs free energy [Ha per Al_2O_3] of the four systems at 298 K (liquid water) and 373.2 K (gas water)

	H_2O	Al_2O_3	B	G	Δ(G–B)
E_{el}	−76.414706· 3	−710.935886	−940.259501	−940.263266	−0.003765
ZPE	0.0211153· 3	0.0170172	0.0959707	0.0965594	0.000588
$\mathscr{H}^{(0,298)}$	0.0028341· 3	0.0036778	0.0087752	0.0084788	−0.000296
$T\mathscr{S}(298)$	0.0079349· 3$^{(1)}$	0.0054872	0.0142384	0.0137140	−0.000524
$\mathscr{G}(298)$	−76.414511· 3$^{(2)}$	−710.920678	−940.168993	−940.171942	−0. 002949
$\mathscr{H}^{(0,373.2)}$	0.0035627· 3	0.0060825	0.0140516	0.0136456	−0.000406
$T\mathscr{S}(373.2)$	0.0274349· 3	0.0095495	0.0237061	0.0229267	−0.000779
$\mathscr{G}(373.2)$	−76.416280· 3$^{(3)}$	−710.922336	−940.173184	−940. 175988	−0.002804

The last column contains the difference between the two polymorphs for each calculated quantity. (1) At T = 298 K the experimental [47] entropy of liquid water must be used; (2) the experimental condensation enthalpy [47] $\Delta\mathscr{H}_{cond} = -0.0167625$ Ha and PV = 0.00094371 Ha have been added to obtain $\mathscr{G}(298)$; (3) PV = 0.0011828 Ha has been added to obtain $\mathscr{G}(373.2)$. 1 Ha = 2625.5 kJ/mol.

As the α-Al_2O_3 unit cell contains 10 atoms only and is much smaller than the B and G ones (56 atoms), its thermodynamic functions have been calculated also from the frequencies of a supercell containing 80 atoms. For reaction 2, $\Delta\mathscr{G}$ shifts by 0.5–1.0 kJ/mol in the 298–450 K interval and T_{inv} shifts by about 1 K.

The individual contributions for corundum and water are shown in Table 3. ZPE gives an important contribution to the energy of all the systems. The other terms, very important for water, are much larger for the hydroxides than for α-Al_2O_3, due to the layered structure and to the presence of the light H atoms. Table 4 shows the Gibbs free energy for the hydration reaction of B and G. In order to compare the computed quantities with experimental data, given at 298 K, where H_2O is liquid, the experimental condensation enthalpy [47] $\Delta\mathscr{H}_{cond}[H_2O]$ = −44.01 kJ/mol and the entropy of the liquid [47], $\mathscr{S}_l[H_2O]$ = 69.91 J mol^{-1} K^{-1}, must be used in the calculation of $\Delta\mathscr{G}(298)$.

The scheme here applied improves the one adopted by Wolverton and Hass [17] and by Digne et al. [15], where the Gibbs free energy of the solid phases was approximated by the electronic energy only (no frequency calculations have been performed) and the $T\mathscr{S}(T)$ and $\Delta\mathscr{H}_{cond}$ contributions were considered for water only.

The experimental $\Delta\mathscr{G}(298)$ values range from −6.54 to −16.16 kJ/mol for G and from −4.01 to −12.16 kJ/mol for B (per Al_2O_3 unit). The present thermodynamic analysis provides $\Delta\mathscr{G}(298) = -12.56$ kJ/mol for B (−14.18 kJ/mol if Wolverton's [17] approximation is adopted) and $\Delta\mathscr{G}(298) = -20.30$ kJ/mol for G (−24.07 kJ/mol with Wolverton's [17] approximation), in quite reasonable agreement with experiment. The results obtained by Digne et al. [15] are 10–20 times larger than the experimental and the present results, and appear completely out of range.

Table 4
$\Delta\mathscr{G}(298)$ per Al_2O_3 unit for bayerite and gibbsite

	B		G	
	$\Delta\mathscr{G}(298)$ (kJ/mol)	T_{inv} (K)	$\Delta\mathscr{G}(298)$ (kJ/mol)	T_{inv} (K)
Experimental				
Werfers [10]	−12.16	450–800	−16.16	450–800
Gitzen [11]	–	573–773	–	573–773
Hemingway [45]	−4.23	–	−14.81	–
Parks [46]	−4.01	–	−9.87	–
Lide [47]	–	–	−6.54	–
Frost [48]	–	–	–	496–576
Calculated				
Digne [15]	−206.8	609	−217.5	624
Wolverton [17]	–	–	−2.7	–
$CRY06_1$ [this Letter]	−14.18	366	−24.07	377
$CRY06_2$ [this Letter]	−12.56	385	−20.30	400

A line separates the experimental (top) from the calculated (bottom) data. T_{inv} is the temperature at which the $Al_2O_3 + 3H_2O$ phases become more stable than B or G. $CRY06_1$ refers to $\Delta\mathscr{G}$ and T_{inv} calculated by neglecting ZPE, $\mathscr{H}^{(0,T)}$ and $\mathscr{S}(T)$ for the solid phases, as in Wolverton [17] and Digne [15] calculations; $CRY06_2$ data are calculated with Eq. (1).

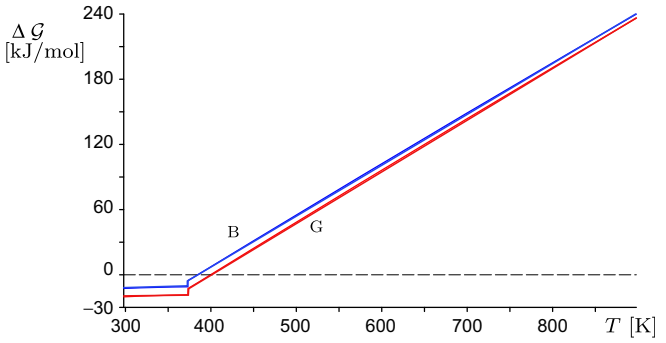

Fig. 4. Calculated stability of gibbsite and bayerite as a function of temperature with respect to $Al_2O_3 + 3H_2O$.

Fig. 4 shows the $\Delta\mathscr{G}$ for B and G as a function of temperature for reaction 2; T_{inv} are reported in Table 4. Our calculated T_{inv} (385 K) is much lower than the proposed experimental values, ranging from 450 to 800 K. The phase transition diagram of the aluminium hydroxide family is however very complicated [10,15,45,11] and the dehydration of $Al(OH)_3$ occurs through various steps, as is confirmed by the experiments performed at different temperatures, defining a quite broad range, rather than a single value for T_{inv}. Kinetic effects are expected to play an important role in the dehydration experimental processes, so that the present calculated T_{inv} must be considered a lower limit for the experimental determinations.

The T_{inv} values obtained by taking into account all the thermodynamic contributions and with Wolverton's [17] approximation differ by about 20 K. As a consequence of the larger $\Delta\mathscr{G}$, Digne's [15] T_{inv} are about 200 K higher than the ones obtained in this work, and fall then in the experimental range.

6. Conclusions

B and G are layered structures, hydrogen bonds being the main contributor to the cohesion among the layers. The main differences between bayerite and gibbsite consist in the sequence by which the layers repeat (ABAB in bayerite, AABBAABB in gibbsite), the position of H atoms and the HB pattern. The structure and the position of H atoms have been optimized and the harmonic stretching frequencies of the six independent OH units have been simulated, in order to investigate the character of the HBs, which can be of intra-layer and inter-layer type.

Intra-layer HBs points towards the triangular-hexagonal cavities present in each layer, and are 2.14–2.30 Å (B) and 2.05–2.29 Å (G) long. Shorter values are obtained for inter-layer HBs,

2.00–2.03 Å (B) and 1.81–1.93 Å (G). Inter-layer HBs are stronger in G than in B: their mean energy has been estimated by computing the isolated layer equilibrium energy; a single inter-layer HB energy is 17.59 and 23.15 kJ/mol in B and G, respectively.

The relative stability and the formation energy with respect to corundum and water have been calculated. Gibbsite is more stable by about 8 kJ/mol than bayerite and the calculated temperatures of dehydration are around 400 K for both.

The results for structure and energy have been compared with experiments, obtaining a satisfactory agreement.

References

[1] R. Demichelis, Y. Noel, B. Civalleri, C. Roetti, M. Ferrero, R. Dovesi, J. Phys. Chem. B 111 (2007) 9337.
[2] Y. Noel, R. Demichelis, F. Pascale, P. Ugliengo, R. Orlando, R. Dovesi, Phys. Chem. Miner. (2008), doi:10.1007/s00269.008.0257.2.
[3] R. Demichelis, Y. Noel, C.M. Zicovich-Wilson, C. Roetti, L. Valenzano, R. Dovesi, J. Phys.: Conf. Ser. 117 (2008) 012013.
[4] H. Liu et al., J. Phys. Chem. B 109 (2005) 8857.
[5] C. Dewey, Am. J. Sci. 2 (1820) 249.
[6] J. Bhöm, Z. Anorg. Allg. Chem. 149 (1925) 203.
[7] R.A.V. Nordstrand, W.P. Hettinger, C.D. Keith, Nature 177 (1956) 713.
[8] G.Y. Chao, J. Baker, A.P. Sabina, A.C. Roberts, Can. Miner. 23 (1985) 21.
[9] H.D. Ruan, R.L. Frost, J.T. Kloprogge, L. Duong, Spectrochim. Acta 58A (2002) 265.
[10] K. Werfers, G.M. Bell, Oxydes and hydroxides of aluminium, ALCOA Technical Paper, N.19, ALCOA Laboratories, Pittsburgh, PA, 1987.
[11] W.H. Gitzen, Alumina as a Ceramic Material, Amer. Ceram. Soc, Columbus, OH, 1970.
[12] A. Chroneos, K. Desai, S.E. Redfern, M.O. Zacate, R.W. Grimes, J. Mater. Sci. 41 (2006) 675.
[13] A. Chroneos, N.J. Ashley, K. Desai, J.F. Maguire, R.W. Grimes, J. Mater. Sci. 42 (6) (2007) 2024.
[14] J.D. Gale, A.L. Rohl, V. Milman, M.C. Warren, J. Phys. Chem. B 105 (2001) 10236.
[15] M. Digne, P. Sautet, P. Raybaud, H. Toulhoat, E. Artacho, J. Phys. Chem. B 106 (2002) 5155.
[16] E. Balan, M. Lazzeri, G. Morin, F. Mauri, Am. Miner. 91 (2006) 115.
[17] C. Wolverton, K.C. Hass, Phys. Rev. B 63 (2) (2001) 024102.
[18] T. Bucheckcko, J. Hafner, J.G. Ángýan, J. Chem. Phys. 122 (2005) 124508.
[19] E. Balan, M. Blanchard, J.F. Hochepied, M. Lazzeri, Phys. Chem. Miner. 35 (2008) 279.
[20] A.D. Becke, J. Chem. Phys. 98 (1993) 5648.
[21] R. Dovesi et al., CRYSTAL 2006 User's Manual, University of Torino, Torino, 2006.
[22] B. Montanari, B. Civalleri, C.M. Zicovich-Wilson, R. Dovesi, Int. J. Quantum Chem. 106 (2006) 1703.
[23] R. Orlando, F.J. Torres, F. Pascale, P. Ugliengo, C. Zicovich-Wilson, R. Dovesi, J. Phys. Chem. B 110 (2006) 692.
[24] F. Pascale, S. Tosoni, C. Zicovich-Wilson, P. Ugliengo, R. Orlando, R. Dovesi, Chem. Phys. Lett. 396 (2004) 308.
[25] F. Pascale, C.M. Zicovich-Wilson, F.L. Gejo, B. Civalleri, R. Orlando, R. Dovesi, J. Comput. Chem. 25 (2004) 888.
[26] M. Prencipe, F. Pascale, C.M. Zicovich-Wilson, V.R. Saunders, R. Orlando, R. Dovesi, Phys. Chem. Miner. 31 (2004) 559.
[27] F. Pascale, C.M. Zicovich-Wilson, R. Orlando, C. Roetti, P. Ugliengo, R. Dovesi, J. Phys. Chem. B 109 (2005) 6146.
[28] F. Pascale, M. Catti, A. Damin, R. Orlando, V.R. Saunders, R. Dovesi, J. Phys. Chem. B 109 (2005) 18522.
[29] S. Tosoni, F. Pascale, P. Ugliengo, R. Orlando, V.R. Saunders, R. Dovesi, Mol. Phys. 103 (18) (2005) 2549.
[30] K. Doll, Comput. Phys. Commun. 137 (2001) 74.
[31] K. Doll, N.M. Harrison, V.R. Saunders, Int. J. Quantum Chem. 82 (2001) 1.
[32] B. Civalleri, P. D'Arco, R. Orlando, V.R. Saunders, R. Dovesi, Chem. Phys. Lett. 348 (2001) 131.
[33] C.G. Broyden, J. I. Math. Appl. 6 (1970) 76.
[34] R. Fletcher, Comput. J. 13 (1970) 317.
[35] D. Goldfarb, Math. Comput. 24 (1970) 23.
[36] D.F. Shanno, Math. Comput. 24 (1970) 647.
[37] S.F. Boys, F. Bernardi, Mol. Phys. 19 (4) (1970) 553.
[38] F. Zigan, W. Joswing, N. Burger, Z. Kristallogr. 148 (1978) 255.
[39] H. Saalfeld, M. Wedde, Z. Kristallogr 139 (1974) 129.
[40] A. Schafer, H. Horn, R. Ahlrichs, J. Chem. Phys. 97 (1992) 2571.
[41] S. Tosoni, K. Doll, P. Ugliengo, Chem. Mater. 18 (8) (2006) 2135.
[42] X. Wu, M.C. Vargas, S. Nayak, V. Lotrich, G. Scoles, J. Chem. Phys. 115 (2001) 8748.
[43] T. Walsh, Phys. Chem. Chem. Phys. 7 (2005) 443.
[44] J.P. Perdew, K. Burke, M. Ernzerhof, Phys. Rev. Lett. 77 (1996) 3865.
[45] B.S. Hemingway, G. Sposito, in: G. Sposito (Ed.), The Environmental Chemistry of Aluminium, CRC Press, Boca Raton, 1995, p. 81.
[46] G.A. Parks, Am. Miner. 57 (1972) 1163.
[47] D.R. Lide, Handbook of Chemistry and Physics, CRC, 1991–1992.
[48] R.L. Frost, J.T. Kloprogge, S.C. Russel, J.L. Szetu, Appl. Spectrosc. 53 (4) (1999) 423.